The Journal of Chemical Physics

Measurement of electron affinity of iridium atom and photoelectron angular distributions of iridium anion

Cite as: J. Chem. Phys. **152**, 034302 (2020); https://doi.org/10.1063/1.5134535
Submitted: 31 October 2019 . Accepted: 29 December 2019 . Published Online: 16 January 2020

Yuzhu Lu, Jing Zhao, Rulin Tang, Xiaoxi Fu, and Chuangang Ning

The Journal of Chemical Physics ARTICLE scitation.org/journal/jcp

Measurement of electron affinity of iridium atom and photoelectron angular distributions of iridium anion

Cite as: J. Chem. Phys. 152, 034302 (2020); doi: 10.1063/1.5134535
Submitted: 31 October 2019 • Accepted: 29 December 2019 •
Published Online: 16 January 2020

Yuzhu Lu,[1] Jing Zhao,[2] Rulin Tang,[1] Xiaoxi Fu,[1] and Chuangang Ning[1,3,a)]

AFFILIATIONS

[1] Department of Physics, State Key Laboratory of Low Dimensional Quantum Physics, Tsinghua University, Beijing 100084, China
[2] Security Printing Institute of People's Bank of China, Beijing 100070, China
[3] Collaborative Innovation Center of Quantum Matter, Beijing, China

[a)] Electronic mail: ningcg@tsinghua.edu.cn

ABSTRACT

The latest electron affinity value of an iridium atom is 1.564 36(15) eV, determined via a method based on the Wigner threshold law by Bilodeau and co-workers. However, they observed a significant deviation from the Wigner threshold law in the threshold photodetachment experiment. To address this dilemma, we conducted high-resolution photoelectron spectroscopy of Ir^- via the slow-electron velocity-map imaging method in combination with an ion trap. The electron affinity of Ir was measured to be 12 614.97(9) cm^{-1} or 1.564 057(11) eV. We find that the Wigner threshold law is still valid for the threshold photodetachment of Ir^- through a p-wave fitting of the photodetachment channel $Ir^-5d^86s^2{}^3F_4 \rightarrow Ir5d^86sb^4F_{9/2}$. The photoelectron angular distributions of photodetachment channels $Ir^-5d^86s^2{}^3F_4 \rightarrow Ir5d^76s^2a^4F_{9/2}$ and $Ir^-5d^86s^2{}^3F_4 \rightarrow Ir5d^86sb^4F_{9/2}$ were also investigated. The behavior of anisotropy parameter β indicates a strong interaction between the two channels. Moreover, the energy level $^3P_2$ of Ir^-, which was not observed in the previous works, was experimentally determined to be 4163.24(16) cm^{-1} above the ground state.

I. INTRODUCTION

Iridium (Ir, atomic number $Z = 77$) is a transition metal in the platinum group. It is the second-densest metal (after osmium) with a density of 22.56 g/cm^3. It is the most corrosion-resistant metal, even at the temperature as high as 2000 °C. The ground state of an Ir atom is $5d^76s^2a^4F$. The electron affinity (EA) of the Ir atom is 1.564 36(15) eV,[1] which is the third-highest EA value (after Pt and Au) in the transition metals, and even higher than EA value 1.461 113 6(9) eV of oxygen.[2] Electron affinity is defined as the energy released when an extra electron is added to a ground-state neutral atom or molecule to form a ground-state anion. It is a fundamental parameter that measures the ability of a neutral atom or molecule to accept an electron and form an anion. The latest EA value 1.564 36(15) eV of the Ir atom was determined via a method based on the Wigner threshold law by Bilodeau and co-workers.[1] However, they observed a significant deviation from the Wigner threshold law in the threshold photodetachment experiment. Therefore, it is worthy to address this dilemma and to measure its EA value again via a different method.

The EA value of Ir was first measured to be 1.566(8) eV by Feigerle *et al.* in 1981 via the laser photoelectron energy spectroscopy (LPES).[3] Later, it was improved by Davies *et al.* in 1997 and by Bilodeau *et al.* in 1999 to be 12 613(4) cm^{-1} or 1.5638(5) eV[4] and 617.4(12) cm^{-1} or 1.564 36(15) eV[1] via the laser photodetachment threshold (LPT) method, respectively. The LPT method determines the electron affinity via a *p*-wave fitting of the experimental data to the Wigner threshold law. In their experiment, Bilodeau *et al.* observed a notable deviation from the *p*-wave Wigner threshold law near the threshold[1] and the deviation could not be explained by any

threshold models at that time. More specifically, for the photodetachment channel $Ir^-5d^86s^{23}F_4 \rightarrow Ir5d^76s^2a^4F_{9/2}$, a p-wave prediction was remarkably lower than the experimental data after the photon energy was ~30 cm^{-1} above the threshold.

In a photodetachment, the Wigner threshold law predicts the behavior of photodetachment cross section near the threshold as[5]

$$\sigma_{\text{tot}} = \begin{cases} a(\varepsilon - \varepsilon_0)^{l+\frac{1}{2}}, & \varepsilon > \varepsilon_0 \\ 0, & \varepsilon \le \varepsilon_0, \end{cases} \quad (1)$$

where σ_{tot} is the total photodetachment cross section, ε is the photon energy, ε_0 is the photodetachment threshold, l is the angular momentum of outgoing photoelectrons, and a is a constant. The Wigner law applies to photodetachment near the threshold, and the energy range of validity is usually much larger than 30 cm^{-1}.[6–9] According to theoretical calculations, Ir^- has three bound states, $^3F_4$, $^3P_2$, and $^3F_3$ with a common configuration $5d^86s^2$ and $^3F_4$ is the anionic ground state.[10] The state $^3P_2$ was not observed by Bilodeau and co-workers,[1] which may cause the deviation. Further experiments are needed to check the validity of the Wigner threshold law for Ir^-.

Another motivation of the present work is to investigate the photoelectron angular distributions (PADs) for detaching a d electron. So far, most PAD studies are focused on the photodetachment of an s or p electron from anions of the main group elements.[11–13] In the present work, we investigated PADs of the photodetachment channel $Ir^-5d^86s^{23}F_4 \rightarrow Ir5d^76s^2a^4F_{9/2}$ at different photon energies. In the case of one-photon ionization or detachment by a linear polarized laser, PAD is given by

$$\frac{d\sigma}{d\Omega} = \frac{\sigma_{tot}}{4\pi}[1 + \beta P_2(\cos\theta)], \quad (2)$$

where σ is the photodetachment cross section, Ω is the solid angle, $P_2(\cos\theta)$ is the second-order Legendre polynomial, $(3\cos^2\theta - 1)/2$, θ is the angle between the velocity of the emitted photoelectron and the electric field of the laser, and β (varies from −1 to 2) is the anisotropy parameter.[14] The anisotropy parameter β can be calculated using the Cooper-Zare equation,[14,15]

$$\beta = \frac{l(l-1)\chi^2_{l,l-1} + (l+1)(l+2)\chi^2_{l,l+1} - 6l(l+1)\chi_{l,l+1}\chi_{l,l-1}\cos(\delta_{l+1} - \delta_{l-1})}{(2l+1)\left[l\chi^2_{l,l-1} + (l+1)\chi^2_{l,l+1}\right]}, \quad (3)$$

where $\chi_{l,l\pm1}$ are the radial matrix elements for the $l \pm 1$ partial waves and $(\delta_{l+1} - \delta_{l-1})$ is the phase shift induced by interaction with the remaining neutral (or cation). The radial matrix elements can be directly calculated.[11–13] Since Eq. (3) shows that β is dependent on the ratio of $\chi_{l,l+1}$ to $\chi_{l,l-1}$, Hanstorp *et al.* proposed a simplification of the problem, assuming that the relative scaling of the partial-wave cross sections follows the Wigner threshold law, i.e., $\chi_{l,l+1}/\chi_{l,l-1} = A_l\varepsilon$,[16] where A_l is a proportionality coefficient and ε is the photoelectron kinetic energy. It is found that the approach of Hanstorp *et al.* is valid over a much broader energy range than the Wigner law.[17]

In this work, we employed the slow-electron velocity-map imaging (SEVI) method[18–20] to measure the EA value of Ir and PAD of Ir^-. SEVI has a very high energy resolution near the photodetachment threshold. We have used this method to determine the EA values of several transition elements with an uncertainty typically less than 1 cm^{-1}.[21–24] Another advantage of the photoelectron imaging method is its ability to measure the photoelectron angular distributions simultaneously.

II. EXPERIMENTAL SETUP

Our SEVI apparatus has been described in detail elsewhere.[21,25–27] Briefly, Ir^- ions are generated by a laser ablation ion source. The anions are trapped and accumulated in an octupole radiofrequency ion trap, which is mounted on the second stage of a liquid helium refrigerator with a variable temperature 5–300 K.[28,29] The trapped ions lose their energy through collisions with the buffer gas (helium in this work). After stored in the trap for 5–45 ms, anions are ejected out by the pulsed potentials on the end caps of the trap. The anions are then accelerated by a −1000 V high voltage pulse and selected by a mass gate. In the photodetachment zone of the imaging lens, a laser beam with an adjustable wavelength intersects the ion beam orthogonally and photodetaches Ir^-. In the experiment for accurately measuring the EA(Ir) value, we use a tunable dye laser (400–920 nm and linewidth 0.06 cm^{-1} at 625 nm) pumped by using a Quanta-Ray Pro 290 Nd:YAG laser (20 Hz and 1000 mJ/pulse at 1064 nm). A wavelength meter (HighFinesse WS6-600) with an accuracy of 0.02 cm^{-1} is adopted to measure the photon energy. For the PAD experiment, we use the signal or idler output of an optical parametrical oscillator (OPO, 405–709 nm for the signal and 710–2750 nm for the idler) pumped by using a Quanta-Ray Lab 190 Nd:YAG laser. The outgoing photoelectrons are projected onto a phosphor screen behind a set of microchannel plates and recorded by using a charge-coupled device (CCD) camera. The hitting position of each photoelectron is determined via a real-time intensity-weighted centroid program and recorded in an event-counting mode.[25] The spherical shells of photoelectrons have cylindrical symmetry. Therefore, the 3D distributions can be reconstructed from the projected 2D images. In this work, the maximum entropy velocity Legendre reconstruction (MEVELER) method is used for the reconstruction.[30]

III. RESULTS AND DISCUSSION

Figure 1 shows the photoelectron spectra obtained at photon energies $h\nu$ = 12 743.65 cm^{-1} and 15 600.74 cm^{-1}. Seven peaks labeled a–g in Fig. 1(a) were observed. Peak g is related to the transition from the ground state $5d^86s^{23}F_4$ of Ir^- to the ground state $5d^76s^2a^4F_{9/2}$ of Ir, and thus, the binding energy (BE) of peak g is the EA value of Ir. As shown in Fig. 1(b), Peak g becomes much stronger and peaks a–f are barely visible as the photon energy changed from 12 743.65 cm^{-1} to 15 600.74 cm^{-1}. Besides, two new peaks h and i show up. Peak i is related to the transition $Ir^-5d^86s^{23}F_4 \rightarrow Ir5d^86sb^4F_{9/2}$. Since the energy level of $b^4F_{9/2}$ is well known with a high accuracy, peak i can also be used to measure the EA(Ir) value, which can provide a check for the experimental results. Since the measured binding energy of peak d in Fig. 1 has a notable deviation from the expected value according to the assignment, we also recorded the photoelectron spectra of Ir^- and IrH^- at photon energy $h\nu$ = 11 509.65 cm^{-1}, as shown in Fig. 2. This is due to the

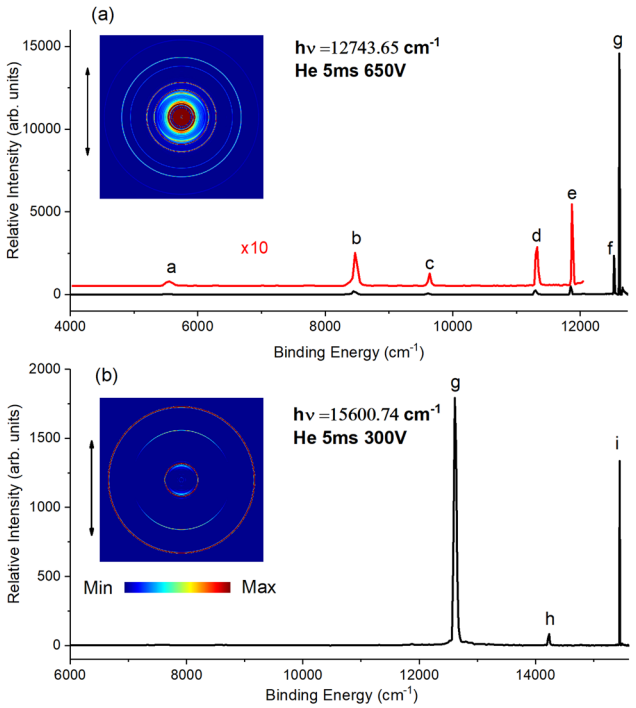

FIG. 1. Photoelectron images and spectra of Ir^- at photon energy $h\nu$ = 12 743.65 cm^{-1}, imaging voltage −650 V (a) and photon energy $h\nu$ = 12 743.65 cm^{-1}, imaging voltage −300 V (b). Ir^- anions are stored in the ion trap for 5 ms, and the buffer gas is helium. The red curve shows the weak peaks multiplied by a factor of 10. The double arrows indicate the polarization of the photodetachment laser.

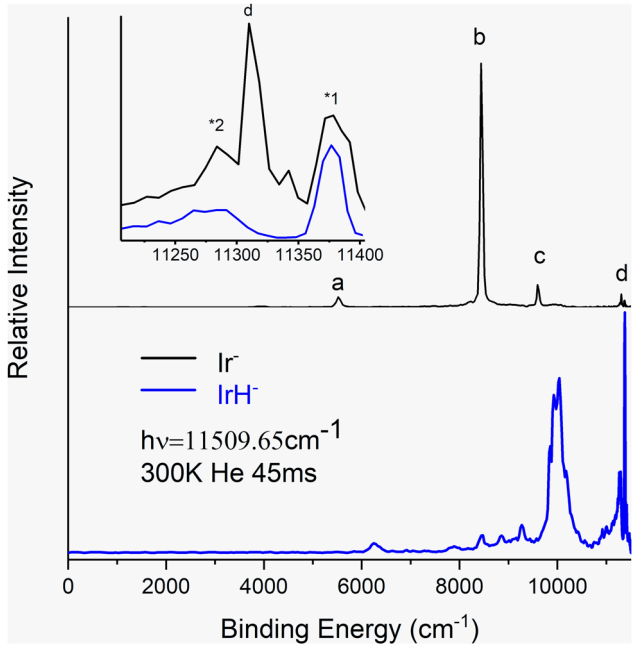

FIG. 2. Photoelectron images and spectra of Ir^- and IrH^- at photon energy $h\nu$ = 11 509.65 cm^{-1} and imaging voltage −650 V. The anions are stored in the ion trap for 45 ms, and the buffer gas is helium. The inset shows the expanded spectra near peak *d*.

appearance of iridium hydride anions IrH^- in our mass spectra. Our mass spectrometer can well resolve the signals of Ir^- and IrH^-. However, in the photodetachment zone, which is ~20 cm behind the mass focus point, there is some mixing of Ir^- and IrH^- due to the out-of-focus effect. As shown in the inset, two extra peaks labeled ^{*1} and ^{*2} are observed, which are due to the contamination of IrH^-. The channel $Ir^-\,^3P_2 \rightarrow Ir b^4F_{9/2}$ (binding energy 11 286.71(14) cm^{-1}) may also contribute partly to peak ^{*2}. It can be seen that the mixing is not significant in Figs. 1 and 2. However, it could have a non-negligible effect on the precise measurement of the center of peak *d* if not resolved. The assignment of all observed peaks is illustrated in Fig. 3.

To determine the binding energy of peak *g* as accurately as possible, a series of spectra were obtained near the threshold of peak *g* at the imaging voltage of −150 V. The photon energy was scanned from 12 629 cm^{-1} to 12 665 cm^{-1} with a step ~10 cm^{-1}. As shown in Fig. 4(a), the binding energy (BE) can be obtained by a linear fitting of experimental data since $h\nu$ = BE + αr^2, where r is the radius of the spherical shell of photoelectrons, α is the slope, and BE is the intercept of the fitting line. As a result, the BE of transition $Ir^-\,^3F_4 \rightarrow Ir a^4F_{9/2}$ is measured to be 12 615.01(11) cm^{-1} or 1.564 062(14) eV. Note that 1 eV = 8065.543 937 cm^{-1}, as recommended by 2018 CODATA (Committee on Data for Science and Technology).[31] The uncertainty includes the statistical uncertainties and the laser linewidth of 0.06 cm^{-1}. For iridium anions with the kinetic energy of 1 keV, the relative correction of photon energy due to Doppler shift is estimated conservatively as 6.0×10^{-7}, resulting in the correction of about 7.6×10^{-3} cm^{-1}.

The binding energy of peak *i* was measured with the same method. The experimental data with a linear fitting are shown in Fig. 5. The binding energy of transition *i* $Ir^-5d^86s^2\,^3F_4 \rightarrow Ir5d^86sb^4F_{9/2}$ is determined to be 15 449.90(12) cm^{-1}. The difference between the binding energies of peaks *g* and *i* is 2834.89(16) cm^{-1}. This is in excellent agreement with the energy level of the excited state $b^4F_{9/2}$ of neutral Ir, which is 2834.98 cm^{-1} above the ground state $a^4F_{9/2}$.[32] The consistency between the two results further confirms the accuracy of our experiment. Once α is known, the binding energies of other peaks can be determined. The energy level of the $^3F_3$ state of Ir^- has been measured as 7087.3(4) cm^{-1} by Thøgersen *et al.*[10] Therefore, the binding energy of $^3F_3$ can be derived since the EA value has been determined. The photodetachment transitions corresponding to the peaks observed in the present work are illustrated in Fig. 3. Since we observed multiple transitions, a global optimization analysis based on covariance algebra was carried out to obtain the interval between two energy levels.[33–35] The measured value of this work, the neutral Ir energy levels,[32] as well as the energy level between $^3F_3$ and $^3F_4$ of Ir^-[10] were utilized for the consistent analysis. The assignment and the binding energy of each peak are listed in Table I.

To check the validity of the Wigner threshold law, we need to measure the photodetachment cross section as the photon energy

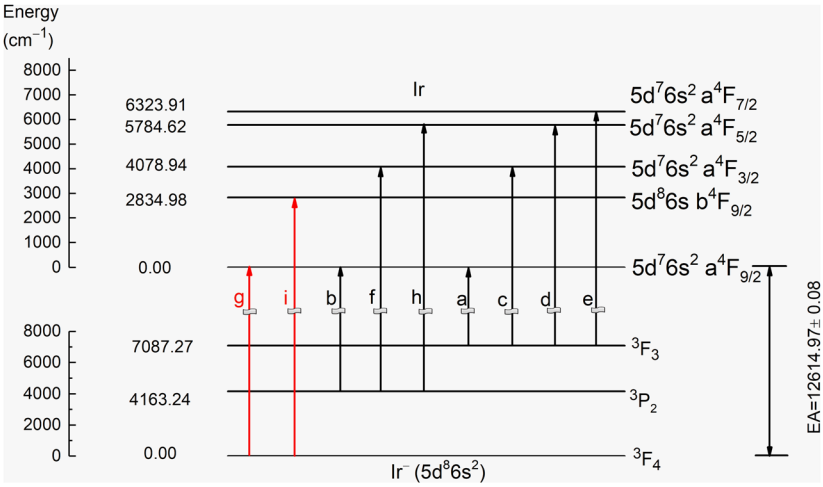

FIG. 3. Partial energy levels of Ir^- and Ir. The labels of transitions are the same as the indexes of the peaks in Fig. 1.

changes. Since the intensities of anion beams and laser beams fluctuate, we measure the ratio of the intensity of peak *i* to that of peak *g* as the relative cross section of transition *i*. When the photon energy varies near the threshold of peak *i*, the varied range is much smaller than the kinetic energies of the photoelectrons from transition *g* (~3000 cm^{-1}). Therefore, it is reasonable to assume that the photodetachment cross section of transition *g* is constant. A series of spectra were obtained near the threshold of transition *i*. As shown in Fig. 6, a *p*-wave fitting [$l = 1$ in Eq. (1)] determines the threshold of transition $Ir^- 5d^8 6s^2 {}^3F_4 \rightarrow Ir 5d^8 6s b^4F_{9/2}$ to be 15 450.22(40) cm^{-1}. Here, the uncertainty includes the statistical uncertainty and the laser linewidth of 0.06 cm^{-1}. This result agrees well with our results obtained via the SEVI method. No obvious deviation from the Wigner threshold law was observed for photodetachment channel *i*. It should be noted that the transition chosen for the LPT experiment of Bilodeau and co-workers is channel *g*. The

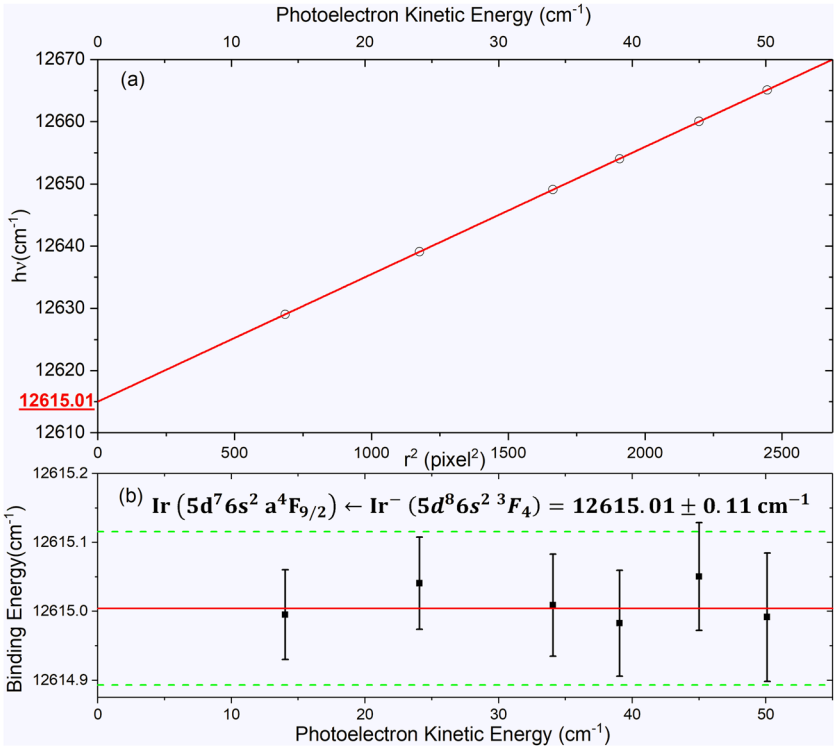

FIG. 4. The photon energy $h\nu$ vs the squared radius r^2 of the photoelectron spherical shell for transition *g*. The solid line is the linear least squares fitting. The intercept 12 615.01 cm^{-1} is the binding energy of photodetachment channel *g* (a). The binding energy of transition $Ir^- {}^3F_4 \rightarrow Ir a^4F_{9/2}$ as a function of the kinetic energy of photoelectrons. The dashed lines indicate the uncertainty ±0.11 cm^{-1}. The uncertainty of energy calibration parameter α has been considered for each error bar (b).

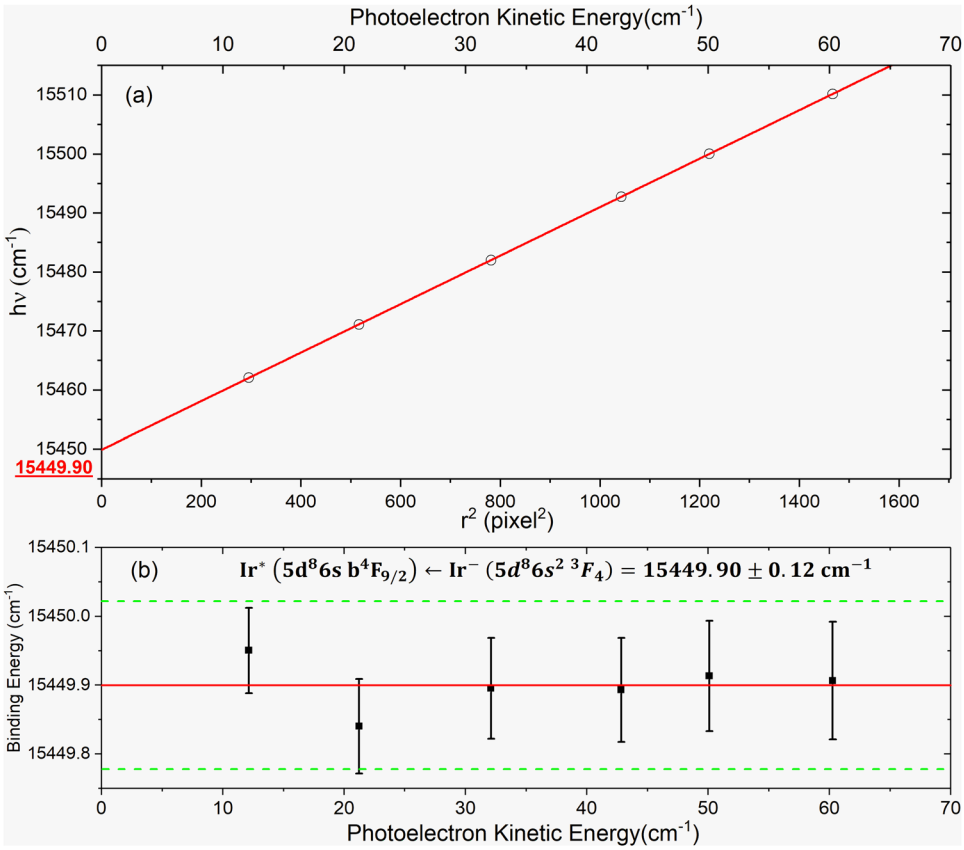

FIG. 5. The photon energy $h\nu$ vs the squared radius r^2 of the photoelectron spherical shell for transition *i*. The solid line is the linear least squares fitting. The intercept 15 449.90 cm^{-1} is the binding energy of photodetachment channel *i* (a). The binding energy of transition $Ir^-\,^3F_4 \rightarrow Irb^4F_{9/2}$ as a function of the kinetic energy of photoelectrons. The dashed lines indicate the uncertainty ± 0.12 cm^{-1}. The uncertainty of energy calibration parameter α has been considered for each error bar (b).

TABLE I. Observed photodetachment transitions and energy levels of Ir^- and the electron affinity of Ir.

Peak	Transition $Ir^- \rightarrow Ir$	Measured binding energy (cm^{-1})	Optimized value (cm^{-1})
a	$^3F_3 \rightarrow a^4F_{9/2}$	5 529(12)	5 527.71(34)
b	$^3P_2 \rightarrow a^4F_{9/2}$	8 448.2(56)	8 451.73(14)
c	$^3F_3 \rightarrow a^4F_{3/2}$	9 607.0(38)	9 606.65(34)
d	$^3F_3 \rightarrow a^4F_{5/2}$	11 312.56(72)	11 312.33(34)
e	$^3F_3 \rightarrow a^4F_{7/2}$	11 851.36(98)	11 851.62(34)
f	$^3P_2 \rightarrow a^4F_{3/2}$	12 530.66(13)	12 530.67(13)
g	$^3F_4 \rightarrow a^4F_{9/2}$	12 615.01(11)	12 614.97(9)
h	$^3P_2 \rightarrow a^4F_{5/2}$	14 236.58(53)	14 236.36(15)
i	$^3F_4 \rightarrow b^4F_{9/2}$	15 449.90(12)	15 449.95(9)

States	Energy level (cm^{-1})	Reference 10
$^3F_4 \rightarrow {}^3P_2$	4163.24(16)	/
$^3F_4 \rightarrow {}^3F_3$	7087.27(33)	7087.3(4)

Electron affinity (cm^{-1})	Reference
12 631(65)	3
12 613(4)	4
12 617.4(12)	1
12 614.97(9)	This work
12 615.24(40)	This work via Wigner fit

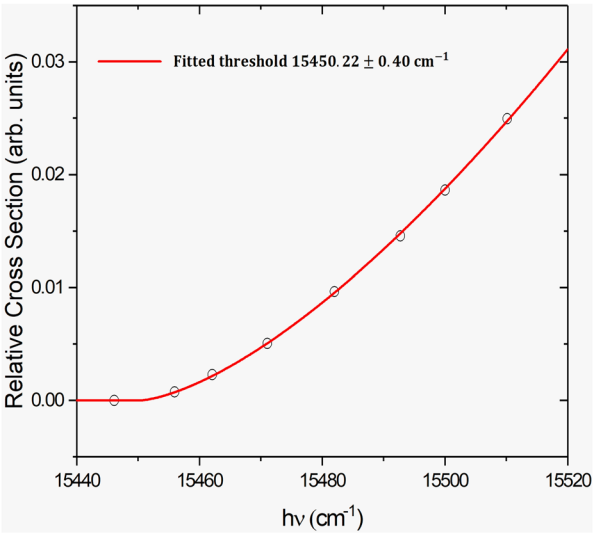

FIG. 6. Relative photodetachment cross section of transition *i* $Ir^-5d^86s^{23}F_4 \rightarrow Ir5d^86sb^4F_{9/2}$ vs the photon energy. The red curve is the *p*-wave Wigner law fitting.

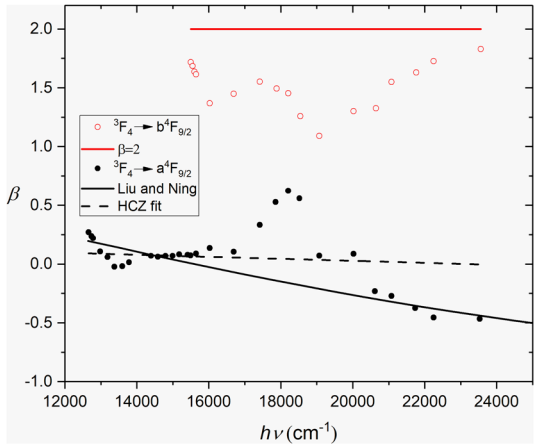

FIG. 7. Anisotropy parameter β for transitions *g* and *i*. The experimental data and the line in red are for transition *i* ($Ir^-5d^86s^{23}F_4 \rightarrow Ir5d^86sb^4F_{9/2}$) and black for transition *g* ($Ir^-5d^86s^{23}F_4 \rightarrow Ir5d^76s^2a^4F_{9/2}$). The black solid line is a result of DFT calculations based on the method of Liu and Ning.[13] The dashed curve is a fitting according to the formulation of the Cooper-Zare equation (HCZ) of Hanstorp *et al.* See the texts for details.

deviation observed by them may be due to the neighboring transition *f*, $Ir^-5d^86s^{23}P_2 \rightarrow Ir5d^76s^2a^4F_{3/2}$, which has a binding energy of 12 530.67(13) cm^{-1}, lying 84.30(15) cm^{-1} below the threshold of transition *g*. The transition *f* is a *p*-wave detachment, and its cross section increases slowly as photon energy increases. The LPT method has a poor ability to distinguish two adjacent *p*-wave photodetachment channels due to a slowly growing slope. In their curve fitting, transition *f* was not considered. This can also explain the disagreement between the EA value 12 617.4 ± 1.2 cm^{-1} by Bilodeau *et al.* and 12 614.97 ± 0.09 cm^{-1} by us.

Figure 7 shows the anisotropy parameter β of peaks *g* and *i* plotted against the photon energy. It should be pointed out that the counting rate of photoelectron signals must be controlled to a relatively low level to avoid the piled-up problem near the photodetachment threshold since the radius of the spherical shell of photoelectrons is very small. The detachment channel *g* is a *d*-electron detachment, and we expect the detached electron to be a superposition of *p*-wave and *f*-wave. For a *d*-electron detachment, the formulation of the Cooper-Zare equation of Hanstorp *et al.* becomes

$$\beta = \frac{2\left(1 + 6A_3^2\varepsilon^2 - 18A_3\varepsilon\cos(\delta_3 - \delta_1)\right)}{5\left(2 + 3A_3^2\varepsilon^2\right)}, \quad (4)$$

where $A_3 = \chi_{2,3}/\varepsilon\chi_{2,1}$, ε is the photoelectron kinetic energy, and $(\delta_3 - \delta_1)$ is the phase shift. However, as Fig. 7 shows, Eq. (4) cannot explain the observed trend of β. To interpret the observed PADs, we also calculated β values via the method based on the density functional theory by Liu and Ning,[13] which also fails to explain the hump around photon energy $h\nu = 18\,000$ cm^{-1}, as shown in Fig. 7. The anomalous behavior of PAD may be due to the configuration interaction between $Ir5d^76s^2a^4F$ and $Ir5d^86sb^4F$.[3] Because of the mixing of $a^4F_{9/2}$ and $b^4F_{9/2}$, channel *g*, $Ir^-5d^86s^{23}F_4 \rightarrow Ir5d^76s^2a^4F_{9/2}$, is a superposition of *s*- and *d*-electron detachment, instead of a pure *d*-electron detachment. Channel *i*, $Ir^-5d^86s^{23}F_4 \rightarrow Ir5d^86sb^4F_{9/2}$, produces a *p*-wave photoelectron if the coupling of final states is neglected. The anisotropy parameter β is expected to be 2 for a *p*-wave detachment. However, a significant deviation from 2 was observed. For example, β is 1.2 for $h\nu = 19\,000$ cm^{-1}. The deviation from 2 reveals the impurity of the *p*-wave character. As shown in Fig. 7, the β value of channel *g* reaches its maximum at $h\nu = 18\,000$ cm^{-1}, which is very close to the position where the largest deviation from 2 of channel *i* occurs, revealing the interaction between the two channels. A more sophisticated theoretical model is needed to reproduce the observed PADs of Ir^- photodetachment.

IV. CONCLUSION

The electron affinity of iridium was determined to be 12 614.97(9) cm^{-1} or 1.564 057(11) eV. The binding energies of bound states $^3P_2$ and $^4F_3$ of Ir^- were measured to be 8451.73(13) cm^{-1} and 5527.71(34) cm^{-1}, respectively. The *p*-wave fitting of transition $Ir^-5d^86s^{23}F_4 \rightarrow Ir5d^86sb^4F_{9/2}$ confirms the validity of the Wigner threshold law for Ir^-. Moreover, the angular distributions of photodetachment transitions $Ir^-5d^86s^{23}F_4 \rightarrow Ir5d^76s^2a^4F_{9/2}$ and $Ir^-5d^86s^{23}F_4 \rightarrow Ir5d^86sb^4F_{9/2}$ were measured vs the photon energy. The observed photoelectron angular distributions cannot be well reproduced with the current models. The present experimental results can serve as a benchmark for further theoretic investigations of photodetachment of the transition element anions.

ACKNOWLEDGMENTS

This work was supported by the National Natural Science Foundation of China (NSFC) (Grant Nos. 91736102 and 11974199) and the National key R&D program of China (Grant No. 2018YFA0306504).

REFERENCES

[1]R. C. Bilodeau, M. Scheer, H. K. Haugen, and R. L. Brooks, Phys. Rev. A **61**, 012505 (1999).
[2]W. Chaibi, R. J. Peláez, C. Blondel, C. Drag, and C. Delsart, Eur. Phys. J. D **58**, 29 (2010).
[3]C. S. Feigerle, R. R. Corderman, S. V. Bobashev, and W. C. Lineberger, J. Chem. Phys. **74**, 1580 (1981).
[4]B. J. Davies, C. W. Ingram, D. J. Larson, and U. Ljungblad, J. Chem. Phys. **106**, 5783 (1997).
[5]E. P. Wigner, Phys. Rev. **73**, 1002 (1948).
[6]H. Hotop and W. C. Lineberger, J. Chem. Phys. **58**, 2379 (1973).
[7]J. W. Farley, Phys. Rev. A **40**, 6286 (1989).
[8]N. D. Gibson, B. J. Davies, and D. J. Larson, J. Chem. Phys. **98**, 5104 (1993).
[9]D. Calabrese, A. M. Covington, J. S. Thompson, R. W. Marawar, and J. W. Farley, Phys. Rev. A **54**, 2797 (1996).
[10]J. Thøgersen, M. Scheer, L. D. Steele, H. K. Haugen, and W. P. Wijesundera, Phys. Rev. Lett. **76**, 2870 (1996).
[11]C. M. Oana and A. I. Krylov, J. Chem. Phys. **127**, 234106 (2007).
[12]C. M. Oana and A. I. Krylov, J. Chem. Phys. **131**, 124114 (2009).
[13]Y. Liu and C. Ning, J. Chem. Phys. **143**, 144310 (2015).
[14]J. Cooper and R. N. Zare, J. Chem. Phys. **48**, 942 (1968).
[15]J. Cooper and R. Zare, J. Chem. Phys. **49**, 4252 (1968).
[16]D. Hanstorp, C. Bengtsson, and D. J. Larson, Phys. Rev. A **40**, 670 (1989).
[17]A. Sanov, Annu. Rev. Phys. Chem. **65**, 341 (2014).
[18]A. Osterwalder, M. J. Nee, J. Zhou, and D. M. Neumark, J. Chem. Phys. **121**, 6317 (2004).
[19]D. M. Neumark, J. Phys. Chem. A **112**, 13287 (2008).
[20]I. León, Z. Yang, H.-T. Liu, and L.-S. Wang, Rev. Sci. Instrum. **85**, 083106 (2014).
[21]X. Chen and C. Ning, Phys. Rev. A **93**, 052508 (2016).
[22]X. Chen, Z. Luo, J. Li, and C. Ning, Sci. Rep. **6**, 24996 (2016).
[23]X. Fu, Z. Luo, X. Chen, J. Li, and C. Ning, J. Chem. Phys. **145**, 164307 (2016).
[24]X. Chen and C. Ning, J. Phys. Chem. Lett. **8**, 2735 (2017).
[25]R. Tang, X. Fu, and C. Ning, J. Chem. Phys. **149**, 134304 (2018).
[26]R. Tang, X. Chen, X. Fu, H. Wang, and C. Ning, Phys. Rev. A **98**, 020501 (2018).
[27]Y. Lu, R. Tang, X. Fu, and C. Ning, Phys. Rev. A **99**, 062507 (2019).
[28]C. Hock, J. B. Kim, M. L. Weichman, T. I. Yacovitch, and D. M. Neumark, J. Chem. Phys. **137**, 244201 (2012).
[29]X.-B. Wang and L.-S. Wang, Rev. Sci. Instrum. **79**, 073108 (2008).
[30]B. Dick, Phys. Chem. Chem. Phys. **16**, 570 (2014).
[31]See http://physics.nist.gov/constants for the 2018 CODATA Recommended Values of the Fundamental Physical Constants.
[32]J. E. Sansonetti and W. C. Martin, J. Phys. Chem. Ref. Data **34**, 1559 (2005).
[33]L. J. Radziemski, Jr., K. J. Fisher, D. W. Steinhaus, and A. S. Goldman, Comput. Phys. Commun. **3**, 9 (1972).
[34]A. Kramida, Comput. Phys. Commun. **182**, 419 (2011).
[35]R. J. Peláez, C. Blondel, M. Vandevraye, C. Drag, and C. Delsart, J. Phys. B: At., Mol. Opt. Phys. **44**, 195009 (2011).